Electronic Supplementary Information

A 1-to-2 Demultiplexer Hybrid Nanocarrier for Cargo Delivery and Activation

Beatriz de Luis, Alba García-Fernández, Antoni Llopis-Lorente, Reynaldo Villalonga, Félix Sancenón, and Ramón Martínez-Máñez*

1. Chemicals

Tetraethyl orthosilicate (TEOS), *n*-cetyltrimethylammonium bromide (CTABr), sodium hydroxide (NaOH), gold(III) chloride trihydrate ($HAuCl_4 \cdot 3H_2O$), sodium citrate tribasic dihydrate, (3-mercaptopropyl)trimethoxysilane, paraffin wax, 3-mercaptopropionic acid, 4-methylumbelliferyl β-D-galactopyranoside, (3-iodopropyl)trimethoxysilane, benzimidazole, triethylamine, β-cyclodextrin, β-galactosidase from *Aspergillus oryzae*, β-galactose dehydrogenase S of *Pseudomonas fluorescens* from *E. coli*, *N*-(3-dimethylaminopropyl)-*N*'-ethylcarbodiimide hydrochloride (EDC), *N*-hydroxysuccinimide (NHS), D-(+)-lactose monohydrate, β-nicotinamide adenine dinucleotide hydrate (NAD^+), D-(+)-galactose, glucose oxidase from *Aspergillus niger*, 2,2'-azino-bis(3-ethylbenzothiazoline-6-sulfonic acid) diammonium salt (ABTS) and peroxidase from horseradish (HRP) from Sigma-Aldrich and used without further purification.

Sodium sulfate anhydrous, sodium dihydrogen phosphate monohydrate, disodium hydrogen phosphate heptahydrate, ethanol, chloroform, toluene and anhydrous acetonitrile were provided by Scharlau.

For cell culture, Dulbecco's Phosphate Buffered Saline (PBS), Dulbecco's Modified Eagle's Medium (DMEM) - high glucose, Fetal Bovine Serum (FBS) and Hoechst 33342 were purchased from Sigma-Aldrich. Cell proliferation reagent WST-1 was obtained from Roche Applied Science. HeLa human cervix adenocarcinoma cells were purchased from the German Resource Centre for Biological Materials (DSMZ).

2. General methods

Powder X-ray diffraction (PXRD), transmission electron microscopy (TEM), N_2 adsorption-desorption isotherms, UV-visible and fluorescence spectrophotometry, dynamic light scattering (DLS) and elemental analysis techniques were employed for materials characterization. PXRD measurements were performed on a Seifert 3000TT diffractometer

using CuKα radiation at low angles ($1.3 < 2\theta < 8.3$, with steps of 0.04 degrees and 3 seconds for step) and high angles ($35 < 2\theta < 80$ with steps of 0.04 degrees and 1 second for step). TEM images were acquired using a JEOL TEM-1010 Electron microscope working at 100 kV. Additionally, TEM coupled with energy dispersive X-ray spectroscopy (TEM-EDX) was used for element mapping using a JEOL TEM-2100F microscope. DLS studies were performed using a ZetaSizer Nano ZS (Malvern). N_2 adsorption-desorption isotherms were recorded on a Micromeritics TriStar II Plus automated analyzer. Samples were previously degassed at 90 °C in vacuum overnight and measurements were performed at 77 K. UV-visible spectra were recorded with a JASCO V-650 Spectrophotometer. Fluorescence measurements were carried out in a JASCO FP-8500 Spectrophotometer. Elemental analysis was performed using a LECO CHNS-932 Elemental Analyzer. Cell viability measurements were taken with a Wallac 1420 workstation. Confocal microscopy imaging was performed with a Leica TCS SP8 AOBS (Leica Microsystems Heidelberg GmbH) inverted laser scanning confocal microscope.

3. Synthesis of mesoporous silica nanoparticles (MSNs)

1.00 g (2.74 mmol) of *n*-cetyltrimethylammonium bromide (CTABr) was dissolved in 480 mL of deionized water. Then, the pH was basified by adding 3.5 mL of a 2 $mol \cdot L^{-1}$ NaOH solution and the temperature was increased to 80 °C. Next, tetraethyl orthosilicate (TEOS) (5 mL, 22.4 mmol) was added dropwise into the solution. Magnetic stirring was kept for 2 h to give a white suspension. Finally, the solid was isolated by centrifugation, washed several times with water until neutral pH and dried at 70 °C overnight (as-synthesized MSNPs). To obtain the final MCM-41 type mesoporous nanoparticles (MSNs), the as-synthesized solid was calcined at 550 °C in an oxidant atmosphere for 5 h in order to remove the surfactant.

4. Synthesis of gold nanoparticles

Gold nanoparticles were synthesized following the Turkevich-Frens method.[1] 100 mL of a 0.3 mM $HAuCl_4 \cdot 3H_2O$ solution were brought to 135 °C under stirring and refluxing. Then, 1.5 mL of a 1 % sodium citrate solution was added to yield gold nanoparticles of ca. 20 nm. The initially pale-yellow colour turned to purple-black and finally red wine in 10 min. After this, the colloidal suspension was cooled to room temperature under stirring. This protocol was repeated 4 times until obtaining 400 mL of the colloidal gold nanoparticles suspension.

5. Synthesis of Janus Au-mesoporous silica nanoparticles (S0)

180 mg of mesoporous silica nanoparticles (MSNs) were dispersed in 9 mL of an aqueous solution (6.7 % ethanol) followed by addition of *n*-cetyltrimethylammonium bromide (CTABr, 1 μM). The mixture was heated at 75 °C, and then 1 g of paraffin wax was added. Once the paraffin was melted, the mixture was vigorously stirred for 15 min using a homogenizer (Ultra-Turrax T-8, IKA). Then, the mixture was further stirred for 1 h at 75 °C using a magnetic stirrer. The resulting Pickering emulsion was then cooled to room temperature, diluted with 10 mL of methanol and reacted with 200 μL of (3-mercaptopropyl)trimethoxysilane for 3 h. The solid was collected by centrifugation and washed with methanol. For gold attachment, the partially mercapto-functionalized nanoparticles were dispersed in 68 mL of methanol and added over the 400 mL of the colloidal gold nanoparticles suspension previously synthesized. The mixture was stirred overnight at room temperature. Then, the solid was isolated by filtration and exhaustively washed with chloroform and hexane. The solid was dried and ground. This process finally yielded the Janus Au-mesoporous silica nanoparticles (**S0**).

6. Synthesis of S1

For the preparation of **S1**, 60 mg of **S0** were suspended in anhydrous acetonitrile (4 mL) and reacted with 60 μL of (3-iodopropyl) trimethoxysilane for 5.5 h. The solid was isolated by centrifugation, washed with acetonitrile and dried at 70 °C overnight. To functionalize the surface with benzimidazole moieties, 0.25 g of benzimidazole and 990 μL of triethylamine were mixed with 20 mL of toluene and heated for 20 min at 80 °C in order to prepare a saturated solution of benzimidazole. 10 mL of this suspension were added over 60 mg of the previously prepared nanoparticles. The mixture was stirred at 80 °C for three days. Afterward, the benzimidazole-functionalized solid was isolated by centrifugation and washed with toluene. To functionalize the gold face, the resulting solid was suspended in 5 mL of acetonitrile and reacted with 50 μL of 3-mercaptopropionic acid for 1 h. This solid (**S0-benz**) was centrifuged, washed with toluene and with water and dried at 70 °C overnight. Next, the loading process was carried out by suspending the solid in 15 mL of a concentrated solution of 4-methylumbelliferyl-β-D-galactopyranoside hydrochloride in 50 mM phosphate buffer at pH 7.5 (20 mg, 3.9 mM). The mixture was stirred overnight (**S0-MUG**). Then, the loaded support was capped by the addition of 367.5 μL of a 64 $mg \cdot mL^{-1}$ solution of β-cyclodextrin-modified β-galactosidase derivative (β-gal-CD, synthesized as previously reported)[2] to the aqueous loading suspension and stirred overnight. Finally, the solid was centrifuged, washed thoroughly with 50 mM phosphate buffer at pH 7.5 and dried under vacuum. This process yielded solid **S1**.

7. Synthesis of $S1_{enz}$

8 mg of **S1** were suspended in 3 mL of 50 mM sodium phosphate buffer at pH 7.5. Then, 2.5 mg of *N*-(3-dimethylaminopropyl)-*N*'-ethylcarbodiimide hydrochloride (EDC), 2.5 mg of *N*-hydroxysuccinimide (NHS) and 120 µL of the enzyme galactose dehydrogenase were added and the suspension was stirred overnight at 10 °C. The solid was isolated by centrifugation and washed several times with cold 50 mM sodium phosphate buffer (pH 7.5). The resulting **$S1_{enz}$** was kept wet in refrigerator until use.

Nanodevice assembly and operation mechanism

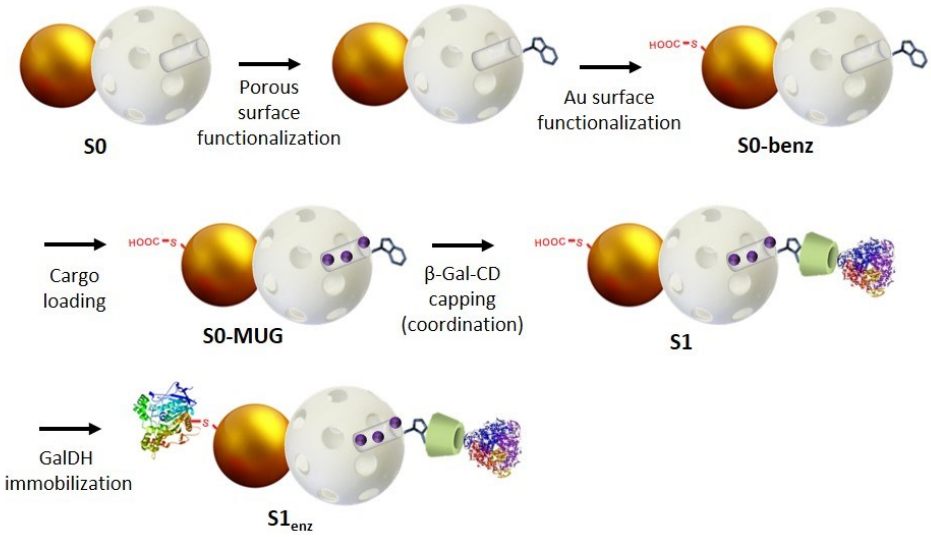

Scheme S1. Illustration of nanodevice assembly.

The assembly of the nanodevice starts with the porous surface functionalization (with benzimidazole moieties) and the Au surface functionalization (with 3-mercaptopropionic acid). Then the loading step consists of suspending the previously obtained functionalizated mesoporous scaffold in a concentrated solution of the cargo in phosphate buffer at pH 7.5. Then this mixture is stirred overnight. Afterwards, the loaded support is capped by adding a solution of β-gal-CD and stirring overnight. The attached benzimidazole and dissolved β-CD forms an inclusion complex (complex formation constant of 104±8 M^{-1})[3] based on Van der Waals forces and hydrophobic interactions[4] which acts as a cap entrapping the payload. Then the solid is isolated by centrifuging and it is intensively washed by several cycles of resuspension and centrifugation in phosphate buffer at pH 7.5 to remove the excess of the cargo present in the solution and also adsorbed into the pore voids which may have not been capped. Despite the excess of the capping ensemble employed and the subsequent washing steps, achieving total capping efficiency is not possible and some residual cargo delivery was

observed (**Figure 1**, main text). As regards the nanodevice operation, upon recognition of the saccharide input, the local pH drops below the pK_a benzimidazole value (pK_a=5.55)[5] due to the generation of galactonic acid by galactose dehydrogenase, causing the protonation of benzimidazole groups. As a result, noncovalent interactions decrease leading to the dissociation of the host-guest complex and provoking the release of the cargo from the pores.

8. Characterization

Solids were characterized by standard techniques.

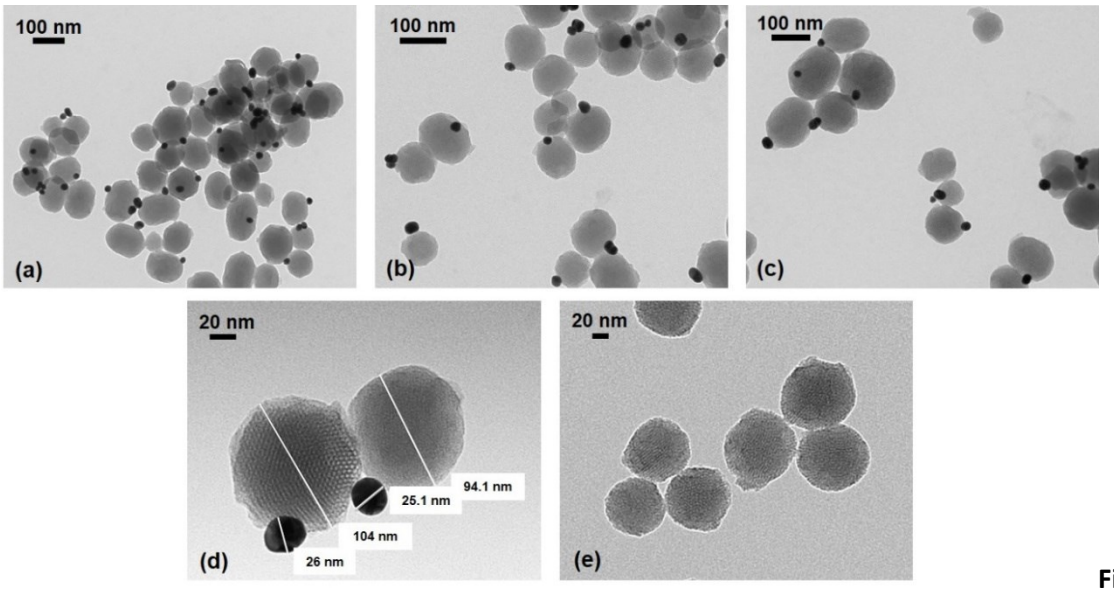

Figure S1. TEM images of (a-d) Janus Au-mesoporous silica nanoparticles **S0** and (e) calcined MSNs.

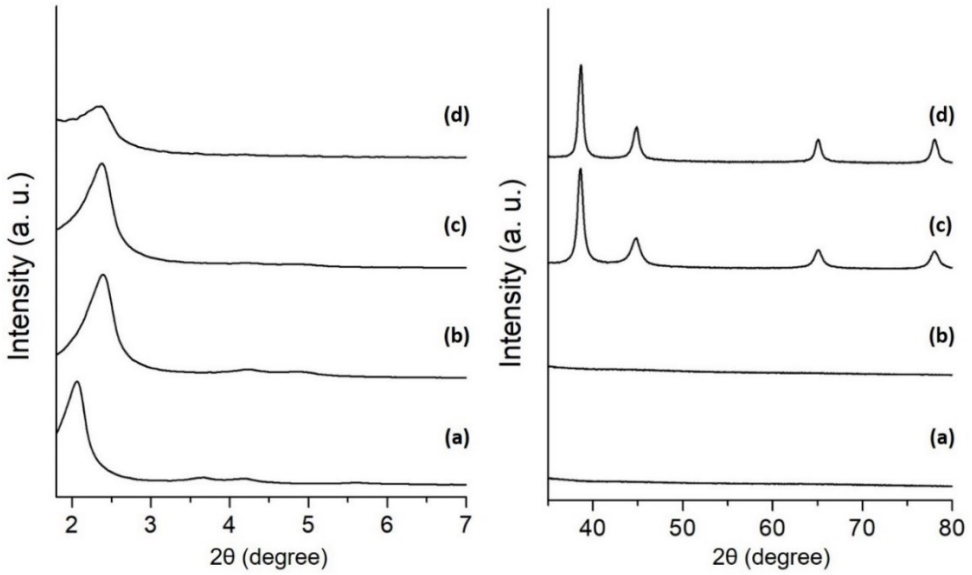

Figure S2. Powder X-ray diffraction patterns of (a) as-made MSNs, (b) calcined MSNs, (c) Janus Au-mesoporous silica nanoparticles **S0** and (d) solid **S1** at low (left) and high (right) angles.

Figure S2 shows the powder X-ray diffraction patterns at low ($1.5 < 2\theta > 7$) and at high angles ($35 < 2\theta > 80$) of as-made MSNs, calcined MSNs, **S0** and **S1**. At low angles, the as-made MSNs (a) shows characteristic low-angle reflections. For the calcined MSNs (b), we observed a slight displacement of the peaks related to the condensation of silanol groups during the calcination process. These low-angle typical peaks are preserved in the Janus Au-mesoporous silica nanoparticles **S0** (c). The presence of the (100) peak in the PXRD patterns in the solid **S1** indicated that the different chemical modifications, functionalization and cargo loading had not damaged the mesoporous structure. Moreover, the high-angle diffraction pattern of the Janus colloids **S0** and **S1** showed the cubic gold characteristic (111), (200), (220) and (331) diffraction peaks, confirming the presence of gold nanocrystals and the Janus Au-MS architecture.[6] Powder X-ray diffraction pattern of $\mathbf{S1}_{\mathbf{enz}}$ was not obtained due to the low quantity collected in the synthesis but the not-harsh enzyme immobilization procedure is not expected to affect the mesoporous structure.

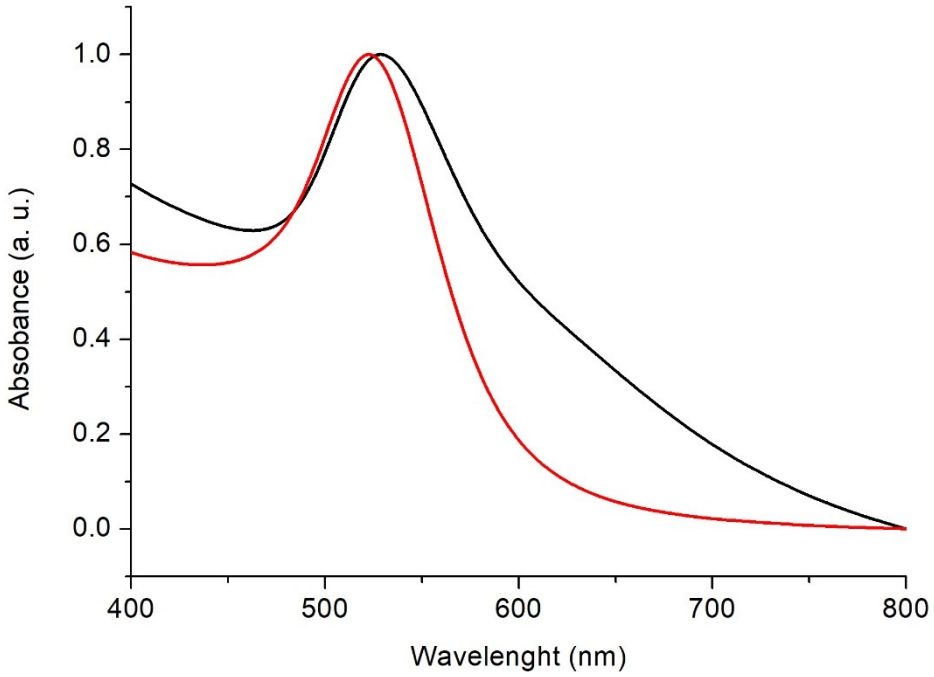

Figure S3. Normalized UV-Visible spectra of the gold nanoparticles (red) and Janus Au-mesoporous silica nanoparticles **S0** (black).

UV/vis measurements in aqueous solution were performed on the as-synthesized gold nanoparticles and on Janus Au-mesoporous silica nanoparticles **S0** (by suspending 1 mg of solid in 1 mL of distilled water). The starting gold colloid shows a single absorption band at 523 nm, characteristic of the surface plasmon resonance of spherically shaped nanospheres with an

approximately 20 nm diameter (**Figure S3**). In the **S0** spectrum, there is a redshift of the absorbance maximum (530 nm) and a broadening of the band (**Figure S3**). These two facts can be ascribed to the increase in the refractive index around the gold nanospheres due to the MSNs attachment and to light refraction produced by silica.[7]

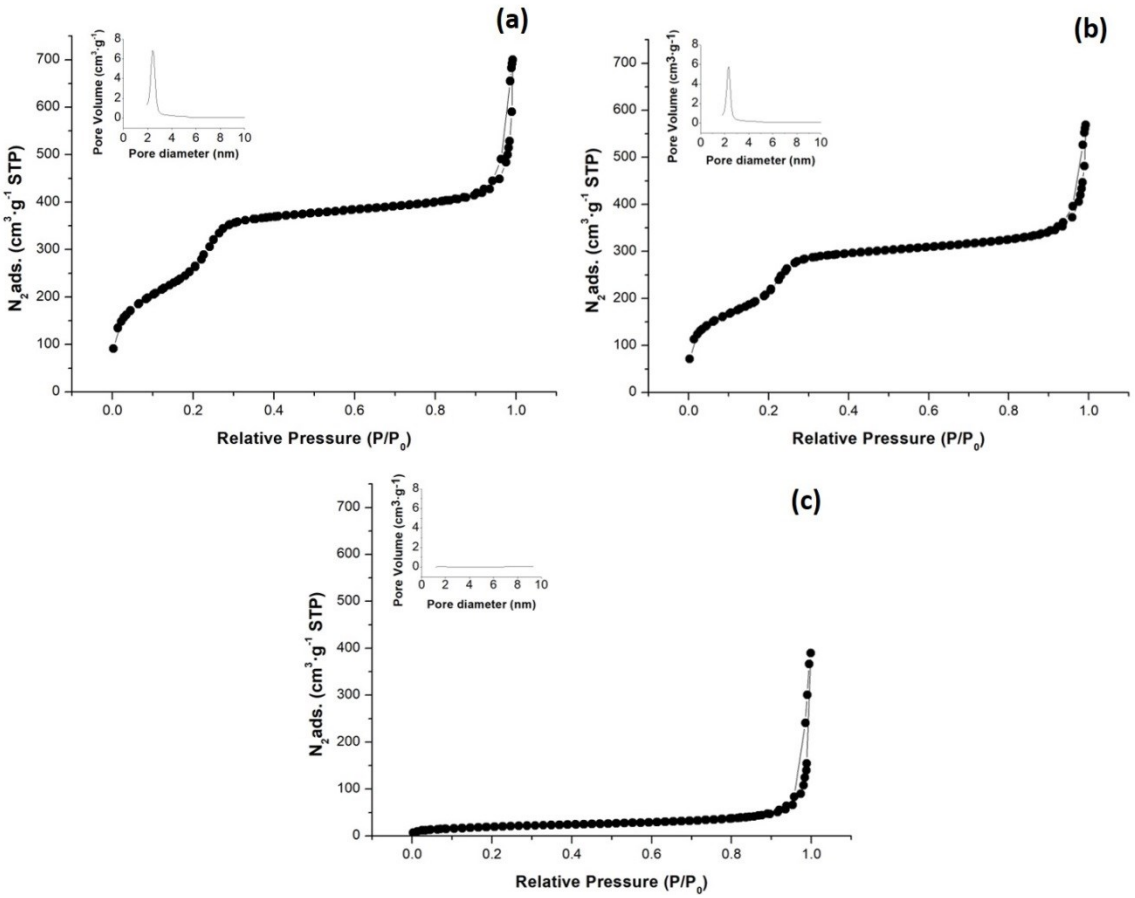

Figure S4. The N_2 adsorption-desorption isotherms for (a) the calcined MSNs, (b) Janus Au-mesoporous silica nanoparticles **S0** and (c) functionalized and loaded solid **S1**.

The N_2 adsorption-desorption isotherms of the calcined MSNs and Janus Au-MS nanoparticles **S0** show an adsorption step at intermediate P/P_0 value 0.3, which is characteristic for mesoporous solids with empty pores (**Figure S4**). This step is related to the nitrogen condensation inside the mesopores by capillarity. The absence of a hysteresis loop in this interval and the narrow BJH pore distribution suggest the existence of uniform cylindrical mesopores. Application of the BET model results in a value for the total specific surface of 960 $m^2 \cdot g^{-1}$ for calcined MSNs and 799 $m^2 \cdot g^{-1}$ for Janus Au-mesoporous silica nanoparticles **S0**. Total specific surface area for **S1** significantly decreased to 74 $m^2 \cdot g^{-1}$ due to the cargo loading inside the mesopores. In order to calculate pore size and total pore volume, BJH model was applied on the adsorption band of the isotherm for $P/P_0 < 0.6$ (associated to adsorption inside the

pores). N_2 adsorption-desorption isotherms for the functionalized and loaded solid **S1** show a significant decrease in N_2 volume adsorbed and are flat when compared (at the same scale) to those from MSNs and **S0** (**Figure S4**). This indicates that there is a significant pore blocking accordingly the loading and capping processes. BET specific values, pore volumes and pore sizes calculated from N_2 adsorption-desorption isotherms for MSNs, Janus Au-MS nanoparticles **S0** and **S1** are listed in **Table S1**.

Table S1. BET specific surface area, pore volumes and pore sizes calculated from N_2 adsorption-desorption isotherms for selected materials.

Solid	S_{BET} [$m^2 \cdot g^{-1}$]	Pore Volume [$cm^3 \cdot g^{-1}$]	Pore size [nm]
Calcined MSNs	960 ± 13	0.70	2.44
S0	799 ± 23	0.56	2.33
S1	74 ± 1	0.05	- -

The zeta potential and hydrodynamic size were also measured by dynamic light scattering (DLS) (**Table S2** and **Figure S5**, respectively). For carrying out the experiments, the corresponding materials were suspended in distilled water at pH 7 at a concentration of 0.01 $mg \cdot mL^{-1}$.

Table S2. Zeta potential values determined by DLS for the different materials.

Sample	Zeta Potential (mV)
MSNs	-34.4 ± 0.6
S0	-33.6 ± 0.8
S0-benz	-29.6 ± 0.5
S1	-42.4 ± 1.4
$S1_{enz}$	-39.7 ± 1.5

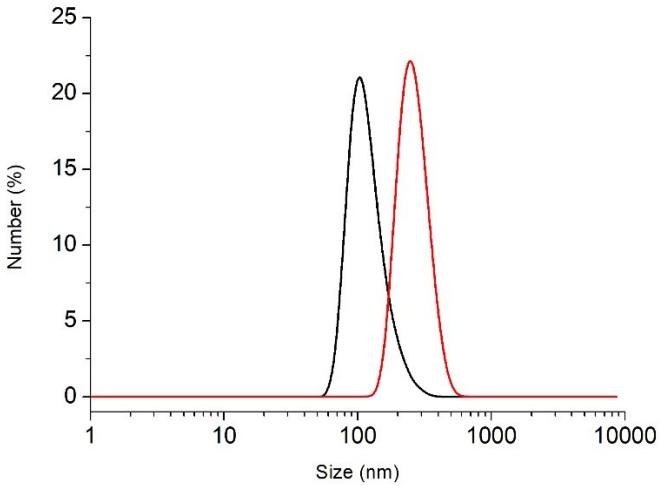

Figure S5. Hydrodynamic diameter distribution (nm) determined by DLS for Janus Au-mesoporous silica nanoparticles **S0** (120 ± 12, black) and final solid **S1$_{enz}$** (265 ± 14, red).

From elemental analysis data (**Table S3**), composition of solids was calculated. Considering the data obtained from the analysis of **S0-MUG** (loaded and functionalized solid), the amount of $(CH_2)_3$-benzimidazole was determined as 18.8 mg·g^{-1} of solid and the cargo 4-methylumbelliferyl β-D-galactopyranoside was estimated to be 171.1 mg·g^{-1}.

Table S3. Elemental analysis data.

Solid	% C	% H	% N
S0	1.84	2.62	0.10
S0-MUG	12.96	2.36	0.33

TEM-EDX mapping of the final nanodevice **S1$_{enz}$** shows the presence of nitrogen atoms in the whole scaffold, which is attributed to the immobilized enzyme (galactose dehydrogenase) in the gold face as well as the benzimidazole moiety of the molecular gate and the enzyme containing β-cyclodextrin derivative (β-galactosidase) in the mesoporous silica face (see **Figure S6**).

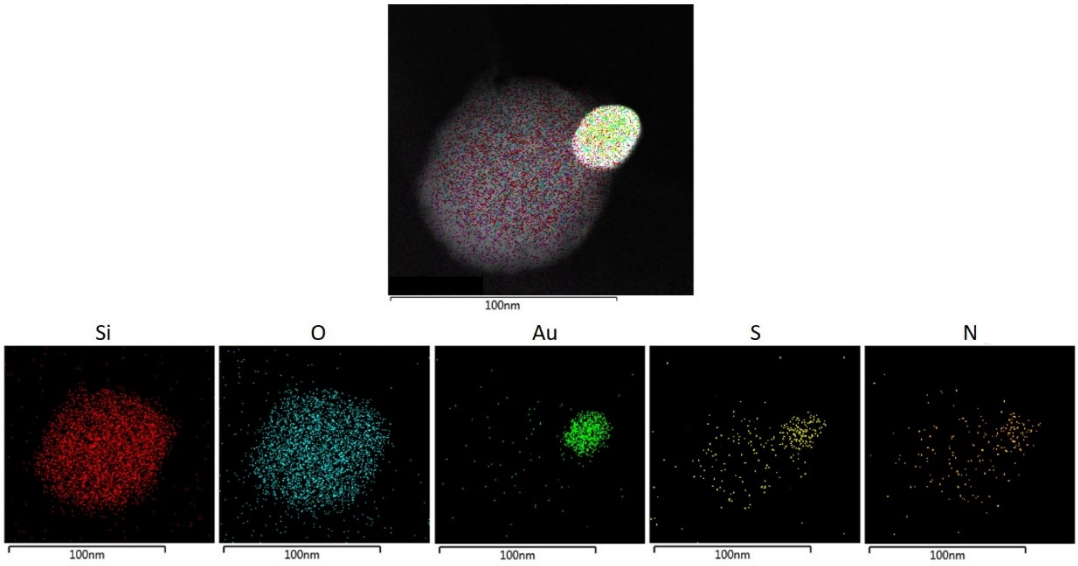

Figure S6. TEM-EDX element mapping of the gold region in the nanodevice **S1$_{enz}$**. Top: mapped area with layered atom composition. Bottom: mapping of different atoms.

In order to confirm the presence of the capping ensemble (β-cyclodextrin), ^{13}C MAS NMR of different solids were carried out. As can be seen in Figure S7, the benzimidazole-functionalized solid (**S0-benz**, red line) shows no aliphatic signals. Moreover, we prepared also the **S0-benz** solid additionally capped with β-cyclodextrin. In this case the ^{13}C MAS NMR spectrum shows a main aliphatic signal at 75 ppm which corresponds to the C-atoms linked to the O-atoms of β-cyclodextrin (blue line) as reported in the literature.[8]

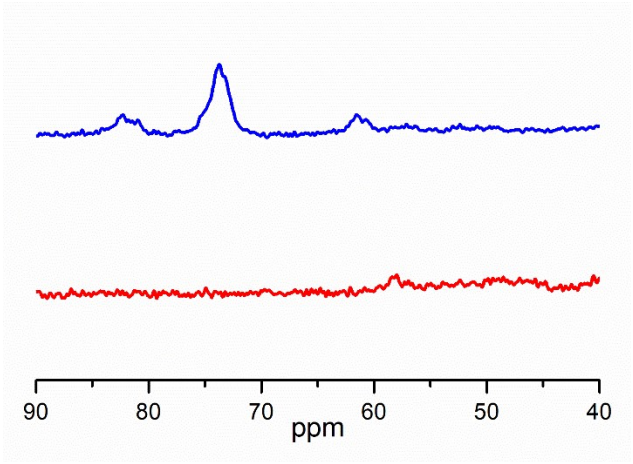

Figure S7. ^{13}C MAS NMR spectra for benzimidazole-functionalized solid (**S0-benz**, red line) and **S0-benz** capped with β-cyclodextrin (blue line).

Functionalization was also assessed by TEM imaging after staining the final nanodevice **S1$_{enz}$** with 1% uranyl acetate. The dark layer around the nanoparticles demonstrates a high coverage with organic matter (Figure S8).

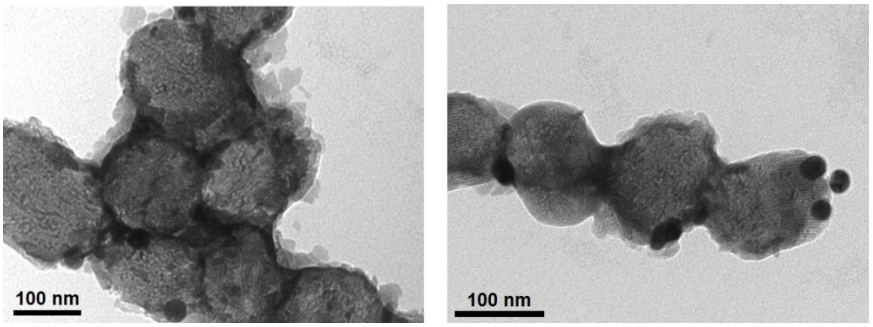

Figure S8. TEM images of **S1$_{enz}$** after staining with 1% uranyl acetate.

9. Enzyme activity assays

The immobilization of β-galactosidase was confirmed by running the corresponding enzyme activity assay and was calculated by applying the following formula:

$$\frac{Enzyme\ Units}{g} = \frac{(\Delta\ -\ \Delta_{blank}) \cdot V_T \cdot F_D}{\mathcal{E}_{chromop.} \cdot l \cdot V_S \cdot C_S}$$

Where, Δ is the slope of the graph (min^{-1}); Δ_{blank} is the slope of the graph for the blank (min^{-1}); V_T is the total volume in the cuvette; F_D is the dilution factor; $\mathcal{E}_{chromop.}$ is the molar extinction of the corresponding chromophore at a defined wavelength (M^{-1}·cm^{-1}); L is the optical path in the cuvette (1 cm); V_S is the volume of the sample added (mL) and C_S is the concentration of sample added (g/mL).

The method we used in order to test β-galactosidase activity is based on the cleavage of lactose by β-galactosidase into galactose and glucose. Then, the glucose is oxidised by glucose oxidase leading to gluconic acid and hydrogen peroxide. Hydrogen peroxide reacts with ABTS (2,2'-azino-bis(3-ethylbenzothiazoline-6-sulfonic acid) diammonium salt) in the presence of peroxidase (HRP) to form a blue-green product (ABTS$^{\cdot+}$) that can be followed UV-visible spectrophotometry (λ_{abs} = 418 nm).

Reactions for assaying β-galactosidase activity are:

$$D\text{-}lactose + H_2O \xrightarrow{\beta\text{-Galactosidase}} D\text{-}glucose + D\text{-}galactose$$
$$D\text{-}glucose + O_2 + H_2O \xrightarrow{\text{Glucose oxidase}} D\text{-}gluconic\ acid + H_2O_2$$
$$H_2O_2 + ABTS \xrightarrow{\text{HRP}} ABTS^{\cdot+} + H_2O$$

In order to check β-galactosidase activity, 250 µL of lactose (5 mg·mL^{-1}), 250 µL of ABTS solution (1 mg·mL^{-1}), 50 µL of glucose oxidase solution (1 mg·mL^{-1}) and 50 µL of HRP solution (2 mg·mL^{-1}) were placed in a quartz cuvette. All solutions had been prepared in 50 mM sodium phosphate buffer at pH 7.5. Then, 10 µL of either buffer (for blank), commercial enzyme solution in buffer (5 mg·mL^{-1}) or **S1$_{enz}$** suspension (5 mg·mL^{-1}) were added. The mixture was shaken and absorbance at 418 nm was monitored as a function of time. Whereas no change was observed in the absence of nanoparticles or commercial enzyme, a strong blue-green colour appeared in the presence of those. The increase in absorbance (ABTS$^{\cdot+}$ formation) as a function of time in the presence of **S1$_{enz}$** and the commercial enzyme solution is depicted in **Figure S7**. After applying the previously indicated formula (ε_{ABTS} at 418 nm = 36,000 M^{-1}·cm^{-1}), the activity of β-galactosidase on **S1$_{enz}$** and the activity of commercial β-galactosidase was determined. From this data, the quantity of enzyme per g of solid was inferred.

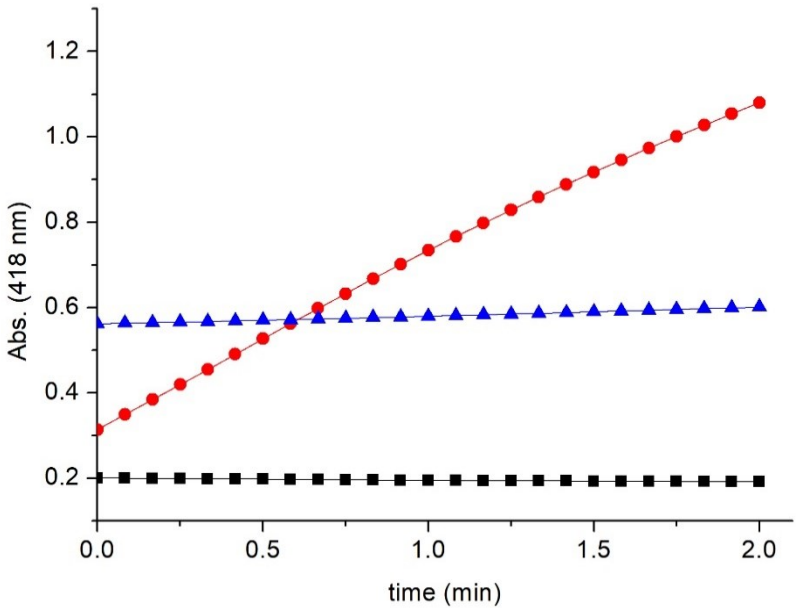

Figure S9. Monitoring of absorbance at 418 nm (ABTS$^{\cdot+}$ formation) due to β-galactosidase activity on nanoparticles **S1$_{enz}$** (blue), enzyme solution (red) and blank (black).

Table S4. Summary of the β-galactosidase activity assays

β-gal on S1$_{enz}$	0.007 U per mg of solid
Commercial β-gal	0.131 U per mg of commercial enzyme
51 mg of β-galactosidase per g of **S1$_{enz}$**	

The immobilization of galactose dehydrogenase was also confirmed by testing its activity. This assay is based on the production of the fluorescent species NADH (reduced β-nicotinamide adenine dinucleotide) by galactose dehydrogenase which can be followed using Fluorescence spectrophotometry (λ_{exs} = 340 nm; λ_{em} = 460 nm).

Reaction for assaying galactose dehydrogenase activity is:

$$D\text{-}galactose + NAD^{+} \xrightarrow{\text{Galactose dehydrogenase}} D\text{–}galactono\text{–}\gamma\text{–}lactone + NADH + H^{+}$$

In order to check galactose dehydrogenase activity, 250 µL of galactose 1 M (180 mg·mL^{-1}), 25 µL of NAD^{+} 20 mM solution (13.25 mg·mL^{-1}) and 475 µL of 50 mM sodium phosphate buffer at pH 7.5 were placed in a black walled cuvette. All solutions had been prepared in 50 mM sodium phosphate buffer at pH 7.5. Then, 5 µL of either buffer (for blank), commercial enzyme or **S1$_{enz}$** suspension (5 mg·mL^{-1}) were added. The mixture was incubated shaking for 2 min, centrifuged and fluorescence at 460 nm was measured. A negligible fluorescent signal was observed in the absence of nanoparticles or commercial enzyme (**Figure S8**). However, emission bands, with a maximum located at 460 nm, for commercial enzyme and **S1$_{enz}$** suspension is observed (**Figure S8**). Considering the specifications of the commercial enzyme (80 U per mg of protein; bottle of 200 U·mL^{-1}), the activity of the nanoparticles was determined by proportionality.

Table S5. Summary of the galactose oxidase activity assays

GalDH on S1$_{enz}$	1.052 U per mg of solid
Commercial GalDH	80 U per mg of commercial enzyme
13 mg of galactose dehydrogenase per g of **S1$_{enz}$**	

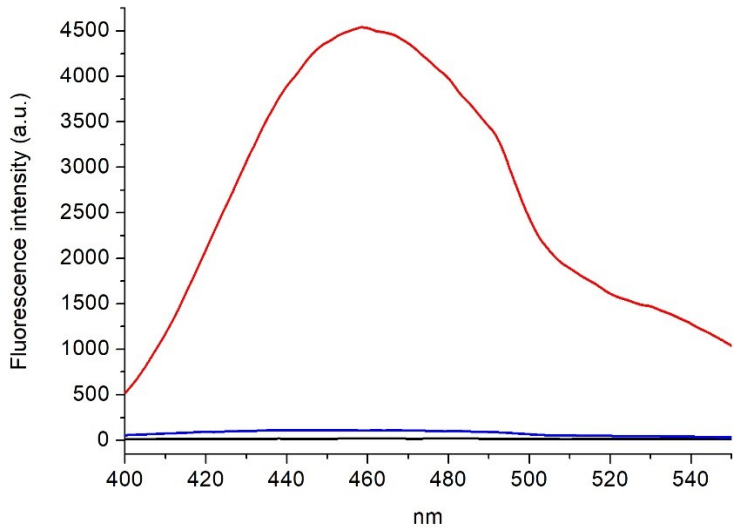

Figure S10. Fluorescent signals of NADH due to galactose dehydrogenase activity on nanoparticles **S1$_{enz}$** (blue), commercial enzyme (red) and blank (black).

From the data obtained (51 mg of β-galactosidase and 13 mg of galactose dehydrogenase per g of S1$_{enz}$) and considering the molecular weight of both enzymes (βGal from *Aspergillus oryzae* = 110 kDa and GalDH from *Pseudomonas fluorescens* = 66 kDa)[9,10] and the equality Da=g·mol^{-1}, we can establish that the molecular ratio of both enzymes in **S1$_{enz}$** is approximately 7:3 (βGal:GalDH).

10. Release studies

Controlled release kinetic profile

For release experiments from **S1$_{enz}$**, the corresponding refrigerated solution of nanoparticles was washed with an aqueous solution (pH 7.5, 20 mM Na_2SO_4), divided into two fractions and brought to a final concentration of 1 mg·mL^{-1}. Both fractions were incubated shaking for 1 h. Then, the inputs (lactose + NAD^+) were added to a fraction (sample) while the same volume of aqueous solution was added to the other fraction (blank). The addition of the inputs was considered as the beginning of the release experiment (time = 0 min). Samples were shaken over time and aliquots were taken at scheduled times, centrifuged (2 min, 12000 rpm) to remove the nanoparticles and the fluorescence was measured (4-methylumbelliferone λ_{exc} = 365 nm, λ_{em} = 445 nm). Error bars in **Figure 1** (main text) correspond to the s.d. from three independent experiments.

Specificity experiments

For specificity experiments of **S1$_{enz}$**, the corresponding refrigerated solution of nanoparticles was washed with an aqueous solution (pH 7.5, 20 mM Na_2SO_4), divided into six fractions and brought to a final concentration of 1 mg·mL^{-1}. All fractions were incubated for 1 h. Then, inputs (monosaccharides and disaccharides + NAD$^+$) were added considering this moment as the beginning of the experiment (time = 0 min). Samples were shaken over time and aliquots were taken after 4 h, centrifuged to remove the nanoparticles (2 min, 12000 rpm) and measured (4-methylumbelliferone λ_{exc} = 365 nm, λ_{em} = 445 nm). Error bars in **Figure S11** correspond to the s.d. from three independent experiments.

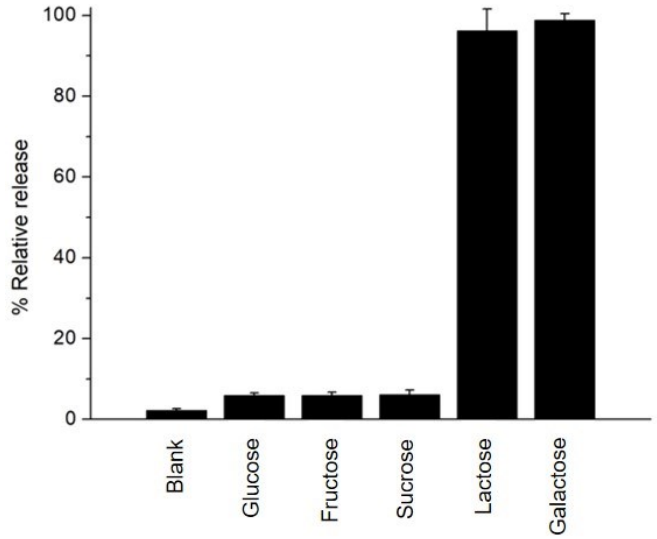

Figure S11. Normalized cargo release from **S1$_{enz}$** in the presence of NAD$^+$ 1 mM and different saccharides at 1 mM after 4 h.

Mechanism studies

In order to confirm the proposed mechanism, two different experiments were carried out:

Enzyme-dependence studies

For mechanism studies, the corresponding refrigerated solution of nanoparticles **S1$_{βGal}$** (only β-galactosidase immobilized), **S1$_{GalDH}$** (only galactosidase dehydrogenase immobilized) and **S1$_{enz}$** were washed with an aqueous solution (pH 7.5, 20 mM Na_2SO_4) and brought to a final concentration of 1 mg·mL^{-1}. Double amount of **S1$_{enz}$** was washed and divided into two fractions to a final concentration of 1 mg·mL^{-1}. All fractions were incubated separately for 1 h. Then, inputs (lactose + NAD$^+$) were added to samples **S1$_{enz}$**, **S1$_{βGal}$** and **S1$_{GalDH}$** while the same volume of aqueous solution was added to the other fraction of **S1$_{enz}$** as a negative control. The addition

of the inputs was considered as the beginning of the experiment (time = 0 min). Samples were shaken for 4 h. Finally, samples were centrifuged (2 min, 12000 rpm) to remove the nanoparticles and the fluorescence was measured (4-methylumbelliferone λ_{exc} = 365 nm, λ_{em} = 445 nm). Error bars in **Figure 2** (main text) correspond to the s.d. from three independent experiments.

MUG β-galactosidase-mediated activation

The refrigerated solution of nanoparticles **S1$_{GalDH}$** (without β-galactosidase enzyme) was washed with phosphate buffer 5 mM at pH 4.5 and divided into two fractions to a final concentration of 1 mg·mL^{-1}. Samples were shaken for 4 h. Then, samples were centrifuged (2 min, 12000 rpm) to remove the nanoparticles and the fluorescence was measured (4-methylumbelliferone λ_{exc} = 365 nm, λ_{em} = 445 nm). After that, 10 µL of β-galactosidase (1 mg·mL^{-1}) were added to one fraction whereas 10 µL of phosphate buffer were added to the other. Samples were shaken for 1 h, centrifuged and the fluorescence was measured (**Figure S12**).

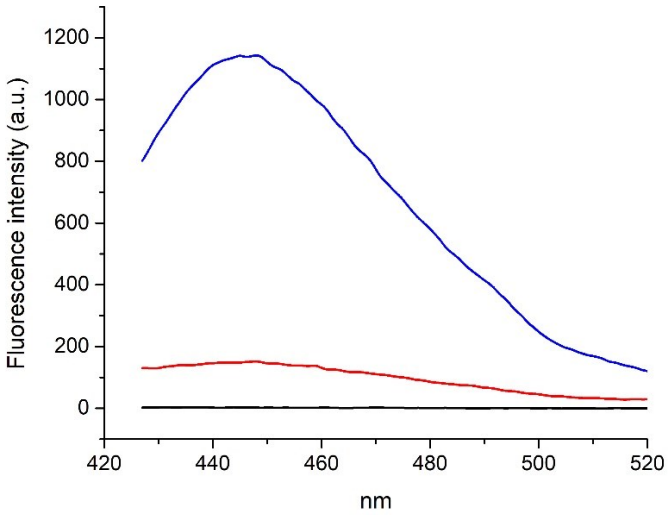

Figure S12. Fluorescent measurements of phosphate buffer 5 mM at pH 4.5 (black), supernatant of **S1$_{GalDH}$** (without β-galactosidase) incubated in phosphate buffer 5 mM at pH 4.5 (red), and supernatant of **S1$_{GalDH}$** (without β-galactosidase) incubated in phosphate buffer 5 mM at pH 4.5 and β-galactosidase (blue).

11. Cell experiments

Cell culture conditions

HeLa human cervix adenocarcinoma cells were purchased from the German Resource Centre for Biological Materials (DSMZ) and were growing in DMEM supplemented with 10% FBS. Cells

were incubated at 37 °C in an atmosphere of 5% carbon dioxide and 95% air and underwent passage twice a week.

Cell viability studies

The biocompatibility of **S1$_{enz}$** solid was tested *in vitro* in the Hela cells. For this purpose, Hela cells were seeded in a 96-well plate at 3500 cells/well and treated with different **S1$_{enz}$** concentrations (0, 25, 50, 100 and 200 μg·mL^{-1} in PBS). Cells were incubated for 24 h and the viability was determined by the WST-1 cell proliferation assay. Finally, the cell viability was measured at λ_{abs} = 595 nm in the Wallac Workstation.

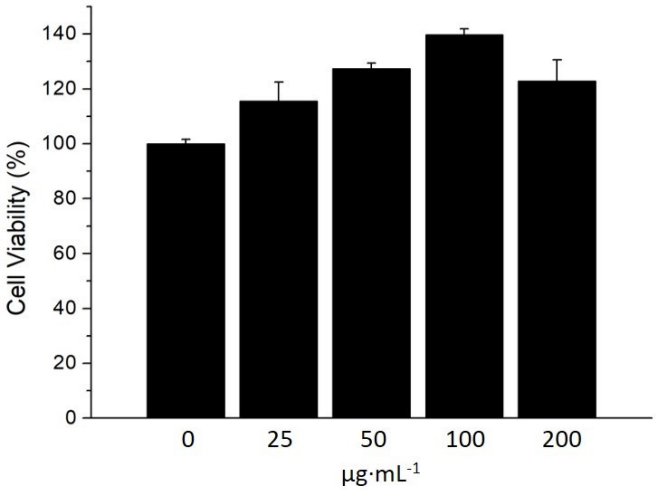

Figure S13. Cell viability studies of HeLa cells treated with different concentrations of **S1$_{enz}$**. Three independent experiments containing triplicates were carried out. Error bars correspond to the s.d.

Controlled release of solid S1$_{enz}$ in HeLa cell line

Internalization and cargo delivery studies using **S1$_{enz}$** were performed in HeLa cells. For this purpose, Hela cells were seeded over glass coverslips at 300000 cells·mL^{-1} in 6-well plate and incubated at 37 °C for 24 h. Then, **S1$_{enz}$** was added to HeLa cells at 75 μg·mL^{-1} and cells were incubated for 1 h. Then cells were washed several times with PBS, new media was added and the nanoparticles were incubated in the absence or presence of lactose for 12 h. After 12 h, cells were washed several times with PBS and, finally, slides were visualized using a confocal microscope Leica TCS SP8 AOBS to follow the MUG release and activation into MUB using an excitation laser at λ_{exc} = 405 nm. Autofluorescence was discarded as no statistically significant differences were found between control and **S1$_{enz}$** treated cells. Three independent experiments were done, which gave similar results. Data in **Figure 3** (main text) are expressed

as mean ± s.e. Statistically significant differences were found between **S1$_{enz}$** and **S1$_{enz}$**+lactose treatments when paired one-way Anova tests were applied (* $p < 0.05$).

As endocytosis is generally the main mechanism of cellular uptake, nanodevices are firstly incorporated into early endosomes, promoting to late endosomes and finally joining lysosomes.[11] Therefore in the first place, fluorescence signals were accumulated in these endocytic compartments or vesicles surrounding perinuclear regions. Once the cargo was released and activated, we observed a remarkable diffused fluorescence pattern throughout the cytosol corresponding, in this case, to cells treated with nanoparticles plus lactose in which more efficient on-command delivery and activation is expected.

12. References

[1] a) J. A. Turkevich, P. C. Stevenson and J. Hillier, *Discuss. Faraday Soc.* 1951, **11**, 55; b) G. Frens, *Nat. Phys. Sci.* 1973, **241**, 20.

[2] a) E. Aznar, R. Villalonga, C. Giménez, F. Sancenón, M. D. Marcos, R. Martínez-Máñez, P. Díez, J. M. Pingarrón and P. Amorós, *Chem. Commun*. 2013, **49**, 6391; b) M. Holzinger, L. Bouffier, R. Villalonga and S. Cosnier, *Biosens. Bioelectron.* 2009, **24**, 1128; c) K. Hamasaki, H. Ikeda, A. Nakamura, A. Ueno, F. Toda, I. Suzuki and T. Osa, *J. Am. Chem. Soc.* 1993, **115**, 5035.

[3] F. O. Yousef, M. B. Zughul and A. A. Badwan, *J. Incl. Phenom. Macrocycl. Chem.* 2007, **57**, 519.

[4] L. Liu, W. -G. Li and G. -X Guo, *J. Incl. Phenom. Macro.* 1999, **34**, 291.

[5] G. Jerez, G. Kaufman, M. Prystai, S. Schenkeveld and K. K. Donkor, *J. Sep. Sci.* 2009, **32**, 1087.

[6] R. Villalonga, P. Díez, A. Sánchez, E. Aznar, R. Martínez-Máñez and J. M. Pingarrón, *Chem. Eur. J.* 2013, **19**, 7889.

[7] K. L. Kelly, E. Coronado, L. L. Zhao and G. C. Schatz, *J. Phys. Chem. B* 2003, **107**, 668.

[8] H. Sfihi, A. P. Legrand, J. Doussot and A. Guy, *Colloids Surf. A Physicochem. Eng. Asp.* 1996, **115**, 115.

[9] M. M. Maksimainen, A. Lampio, M. Mertanen, O. Turunen and J. Rouvinen, *Int. J. Biol. Macromol*. 2013, **60**, 109.

[10] C. F. Mazitsos, D. J. Rigden, P. G. Tsoungas and Y. D. Clonis, *Eur. J. Biochem*. 2002, **269**, 5391.

[11] T.-G. Iversen, T. Skotland and K. Sandvig, *Nano Today* 2011, **6**, 176.